Recent Hypernuclei Measurements in the High Baryon Density Region with the STAR Experiment at RHIC*

Yue Hang Leung, for the STAR collaboration

Heidelberg University

Received July 30, 2022

Hypernuclei are expected to be abundantly produced in intermediate to low energy heavy-ion collisions due to the high baryon density. Measurements of the yield and collective flow are sensitive to their production mechanisms and the dynamics of the produced medium. In particular, hypernuclei measurements may also bear implications on the hyperon-nucleon interaction, which is critical to understanding the nuclear equation of state in high baryon density medium including strangeness degrees of freedom.

The STAR Beam Energy Scan Phase II program, carried out during 2018-2021, is particularly suited for such studies. In this talk, the collision energy dependence of light hypernuclei (${}^{3}_{\Lambda}$H, ${}^{4}_{\Lambda}$H, ${}^{4}_{\Lambda}$He) production yields in $\sqrt{s_{\mathrm{NN}}} = 3.0, 19.6$ and 27.0 GeV Au+Au collisions will be presented. Results on hypernuclei directed flow will also be presented. Furthermore, measurements of hypernuclei lifetimes and relative branching ratios will be reported. The physics implications of our measurements in the context of hypernuclear structure and their production mechanisms will be discussed.

1. Introduction

Nuclei containing at least one hyperon are known as hypernunclei, and they serve as important experimental probes to access the hyperon-nucleon (Y-N) interaction. The Y-N interaction is an important ingredient in the equation-of-state of high baryon density matter, such as neutron stars or the hadronic phase of a heavy-ion collision. Hypernuclei measurements related to their internal structure provide strong constraints on the Y-N interaction, while measurements of their yields and flow in heavy-ion collisions can shed light on their production mechanisms, which is currently not well understood.

* Presented at Quark Matter 2022

2. STAR Beam Energy Scan II and Hypernuclei Reconstruction

In heavy-ion collisions, hypernuclei yields are expected to increase towards lower beam energies due to the increasing baryon density [6]. The STAR Beam Energy Scan II program, which covers collision energies from $\sqrt{s_{\rm NN}} = 3.0$ to $27.0\,\rm GeV$, provides a great opportunity for hypernuclei studies. In the following, we will discuss recent hypernuclei measurements carried out using data from Au+Au collisions at $\sqrt{s_{\rm NN}} = 3.0$, 7.2, 19.6 and $27.0\,\rm GeV$ taken in 2018 and 2019. 258, 155, 478 and 555 million events have been analyzed for each aforementioned dataset respectively. Hypernuclei are reconstructed using their mesonic decay channels, e.g. ${}^{3}_{\Lambda}\rm H \to {}^{3}He + \pi^{-}$ and ${}^{4}_{\Lambda}\rm H \to {}^{4}He + \pi^{-}$. Particle identification of the daughter tracks is achieved by the measured ionization energy loss in the Time Projection Chamber.

3. Probing the Internal Structure of Hypernuclei

3.1. Relative Branching Ratio R_3

The ${}^{3}_{\Lambda}\rm H$ relative branching ratio R_3, defined as:

$$R_3 = \frac{BR({}^{3}_{\Lambda}\rm H \to {}^{3}He + \pi^{-})}{BR({}^{3}_{\Lambda}\rm H \to {}^{3}He + \pi^{-}) + BR({}^{3}_{\Lambda}H \to d + p + \pi^{-})}, \tag{1}$$

where BR stands for branching ratio, has been suggested to be sensitive to the ${}^{3}_{\Lambda}\rm H$ binding energy [1]. The ${}^{3}_{\Lambda}\rm H$ yields are measured in $\sqrt{s_{\rm NN}} = 3.0\,\rm GeV$ Au+Au collisions via both two-body and three-body decay channels, and R_3 can be subsequently determined. The preliminary result $R_3 = 0.27 \pm 0.03(stat) \pm 0.04(syst)$, as shown in Fig. 1, is consistent with previous measurements. The improved precision on R_3 can provide stronger constraints on hypernuclear interaction models.

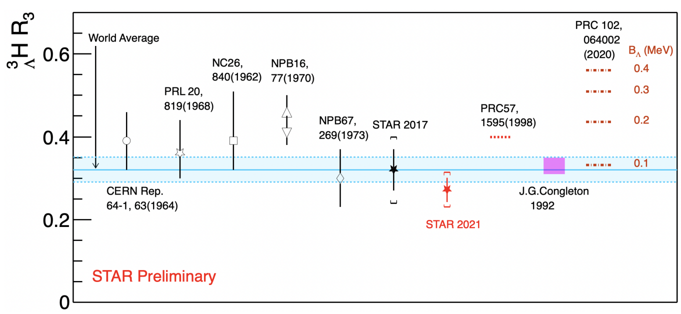

Fig. 1. Compilation of ${}^{3}_{\Lambda}\rm H$ relative branching ratio R_3. The experimental average R_3 is indicated by the blue shaded band. The magenta box and dashed red and orange lines represent theoretical calculations.

3.2. Lifetime

Using $\sqrt{s_{\mathrm{NN}}} = 3.0\,\mathrm{GeV}$ and $7.2\,\mathrm{GeV}$ data taken in 2018, the ${}^{3}_{\Lambda}\mathrm{H}$ and ${}^{4}_{\Lambda}\mathrm{H}$ yields are measured as a function of proper decay length. The lifetimes are extracted via an exponential fit. The ${}^{3}_{\Lambda}\mathrm{H}$ and ${}^{4}_{\Lambda}\mathrm{H}$ lifetimes are measured to be $221 \pm 15(stat) \pm 19(syst)$ and $218 \pm 6(stat) \pm 13(syst)$ respectively [2]. The same methodology is applied to ${}^{4}_{\Lambda}\mathrm{He}$ and the preliminary result of the ${}^{4}_{\Lambda}\mathrm{He}$ lifetime, $229 \pm 23(stat) \pm 20(syst)$, is reported. The results are compared to previous measurements and theoretical calculations in Fig. 2. The experimental averaged ${}^{3}_{\Lambda}\mathrm{H}$ lifetime is $(76 \pm 5)\%$ of the Λ lifetime, and is consistent with theoretical calculations incorporating pion final-state interactions [3]. Meanwhile, the measured ${}^{4}_{\Lambda}\mathrm{H}$ and ${}^{4}_{\Lambda}\mathrm{He}$ lifetimes are consistent with theoretical estimates invoking the isospin rule [4]. The new results have an improved precision compared to previous measurements and are expected to provide stronger constraints to hypernuclear interaction models.

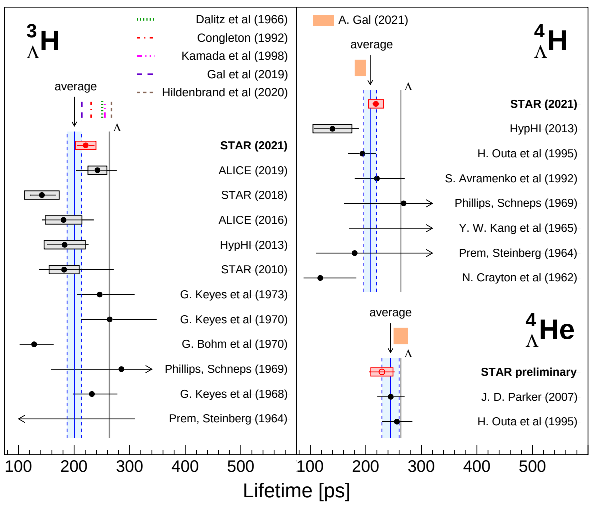

Fig. 2. Compilation of ${}^{3}_{\Lambda}\mathrm{H}$, ${}^{4}_{\Lambda}\mathrm{H}$ and ${}^{4}_{\Lambda}\mathrm{He}$ lifetimes. The experimental average lifetimes are indicated by blue shaded bands. The short dashed lines represent theoretical calculations while the solid grey line indicates the free Λ lifetime.

4. Hypernuclei Production in Heavy-Ion Collisions

4.1. Yield and Particle Ratios

The ${}^{3}_{\Lambda}\mathrm{H}$ yields at $\sqrt{s_{\mathrm{NN}}} = 3.0$, 19.6 and $27.0\,\mathrm{GeV}$ are presented as a function of transverse momentum p_T, rapidity and centrality. The ${}^{4}_{\Lambda}\mathrm{H}$ yield at $\sqrt{s_{\mathrm{NN}}} = 3.0\,\mathrm{GeV}$ is also reported [3]. The mid-rapidity yields in 0–10%

collisions are compared to theoretical calculations and the measured ${}^{3}_{\Lambda}$H yield at $\sqrt{s_{\mathrm{NN}}} = 2.76$ TeV [5]. The ${}^{3}_{\Lambda}$H yield rises as the energy decreases, likely driven by the increasing baryon density. This trend is qualitatively reproduced by thermal model calculations [6], although the yields at $\sqrt{s_{\mathrm{NN}}} = 19.6$ and 27.0 GeV are overestimated. Meanwhile, the same model underestimates the ${}^{4}_{\Lambda}$H yield at $\sqrt{s_{\mathrm{NN}}} = 3.0$ GeV. To investigate further, the ${}^{3}_{\Lambda}$H and ${}^{4}_{\Lambda}$H yields at $\sqrt{s_{\mathrm{NN}}} = 3.0$ GeV are compared to Λ and light nuclei yields at the same energy. As shown in the left panel of Fig. 4, the light nuclei yields, when divided by the spin degeneracy, follow an approximate exponential dependence as a function of the mass number A. However, ${}^{4}_{\Lambda}$H lies a factor of 6 above the exponential fit to the (Λ, ${}^{3}_{\Lambda}$H and ${}^{4}_{\Lambda}$H) yields. As shown in the right panel, a non-monotonic behavior in hypernuclei to light nuclei yield ratio as a function of A is observed. This trend can be qualitatively reproduced by thermal model calculations including feed-down from the excited ${}^{4}_{\Lambda}$H* state [6]. These observations support the creation of excited hypernuclei in heavy-ion collisions.

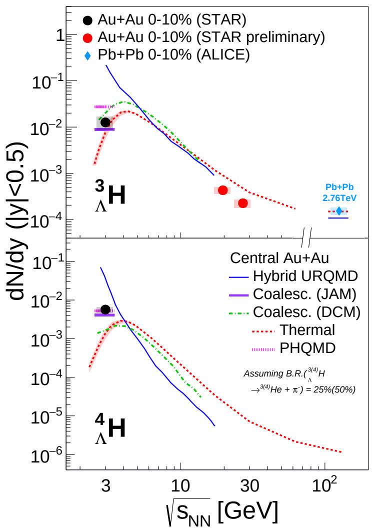

Fig. 3. ${}^{3}_{\Lambda}$H (upper panel) and ${}^{4}_{\Lambda}$H (lower panel) yields within $|y| < 0.5$ as a function of beam energy in central heavy-ion collisions. The symbols represent measurements [2, 5] while the lines represent different theoretical calculations.

The strangeness population factor S_A, defined as [7]:

$$S_A = \frac{{}^{A}_{\Lambda}\mathrm{H}(\mathrm{A} \times \mathrm{p_T})}{{}^{A}\mathrm{He}(\mathrm{A} \times \mathrm{p_T}) \times \frac{\Lambda}{\mathrm{p}}(\mathrm{p_T})}, \quad (2)$$

incorporates the Λ/p ratio in order to remove the absolute difference in Λ and p yields, thus enabling a fair comparison between hypernuclei and light nuclei production. The ratios in different p_T, rapidity, and centrality selections are shown in the left panel of Fig. 5. For both S_3 and S_4, no significant dependence on p_T, rapidity, or centrality is observed.

The integrated S_3 in the kinematic region ($|y| < 0.5$, $p_T/A > 0.4$ GeV/c) is computed for $\sqrt{s_{\mathrm{NN}}} = 3.0$, 19.6 and 27.0 GeV 0–40% Au+Au collisions. As shown in the right panel of Fig. 5, a hint of an increasing trend from $\sqrt{s_{\mathrm{NN}}} = 3.0$ GeV to 2.76 TeV is observed. It has been suggested that an increase in

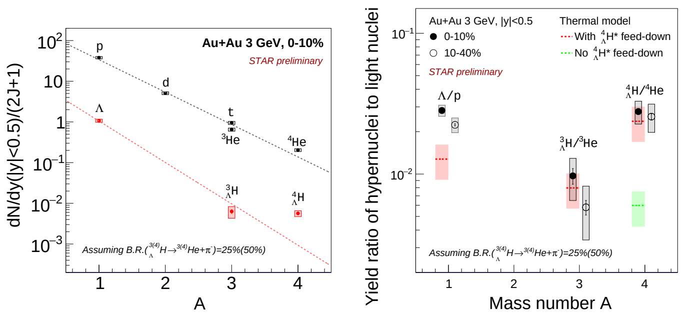

Fig. 4. (left) Light nuclei and hypernuclei yields at $|y| < 0.5$ in $\sqrt{s_{\rm NN}} = 3.0\,$GeV 0–10% collisions as a function of mass number A. The dotted lines represent exponential fits to the data. (right) Ratio of hypernuclei to light nuclei yields as a function of A in $\sqrt{s_{\rm NN}} = 3.0\,$GeV 0–10% (solid symbols) and 10–40% (open symbols) collisions. The red and green dashed bands represent thermal model calculations with and without ${}^4_\Lambda$H* feed-down respectively.

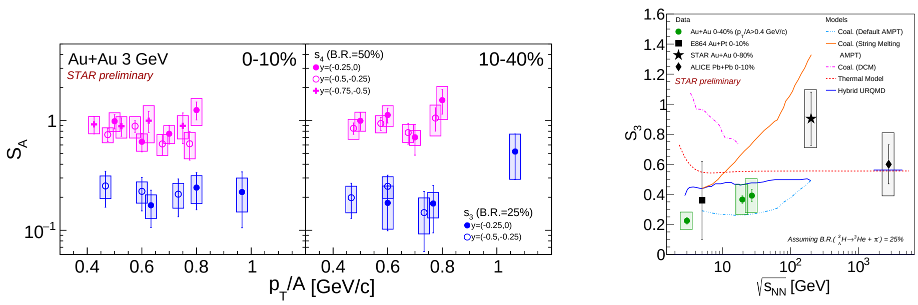

Fig. 5. (left) S_3(blue) and S_4(magenta) as a function of p_T/A in 0–10% and 10–40% $\sqrt{s_{\rm NN}} = 3.0\,$GeV Au+Au collisions. Different markers correspond to different rapidity ranges. (right) S_3 as a function of $\sqrt{s_{\rm NN}}$. The different colored lines represent theoretical calculations.

S_3 as a function of $\sqrt{s_{\rm NN}}$ may be related to the onset of deconfinement [7]. However, none of the models shown describe the S_3 data quantitatively. Future theoretical developments is necessary to help interpret the data.

4.2. Collectivity

The directed flow of hypernuclei and light nuclei in $\sqrt{s_{\rm NN}} = 3.0\,$GeV 5–40% collisions are reported and shown in the left panel of Fig. 6. The hypernuclei v_1 slope, similar to that of light nuclei, follows mass number scaling. The average p_T of hypernuclei and light nuclei in $\sqrt{s_{\rm NN}} = 3.0\,$GeV 0–10% collisions are shown in the right panel of Fig. 6. Similarly, linear trends are observed for hypernuclei and light nuclei, which reflects the dominance of collective radial motion. These results are consistent with hypernuclei production from coalescence of hyperons and nucleons.

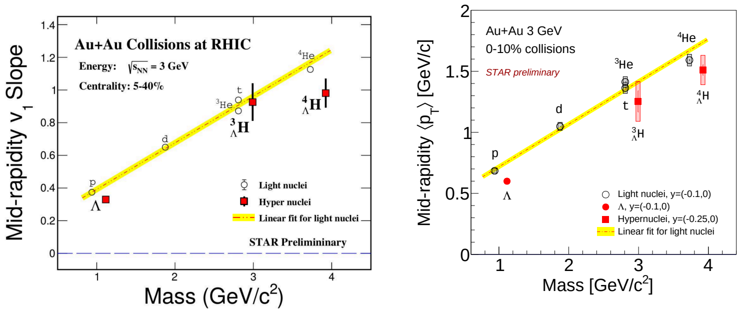

Fig. 6. (left) Hypernuclei and light nuclei dv_1/dy (left) and $\langle p_T \rangle$ (right) at mid-rapidity as a function of mass in $\sqrt{s_{\mathrm{NN}}} = 3.0\,\mathrm{GeV}$ 5–40% and 0–10% collisions respectively. Yellow bands are linear fits to the light nuclei dv_1/dy and $\langle p_T \rangle$.

5. Summary

In summary, the first batch of hypernuclei results from the STAR Beam Energy Scan II Program have been presented. Hypernuclei lifetimes and branching ratios have been measured with improved precision, providing stronger constraints to hypernuclear interaction models. ${}^{3}_{\Lambda}\mathrm{H}$ and ${}^{4}_{\Lambda}\mathrm{H}$ yields at $\sqrt{s_{\mathrm{NN}}} = 3.0\,\mathrm{GeV}$, and the ${}^{3}_{\Lambda}\mathrm{H}$ yield at 19.6 and 27.0 GeV are also presented. At $\sqrt{s_{\mathrm{NN}}} = 3.0\,\mathrm{GeV}$, the yield ratios of hypernuclei to light nuclei follow a non-monotonic trend, which suggests the production of excited ${}^{4}_{\Lambda}\mathrm{H}^{*}$ states. Finally, the directed flow of hypernuclei at $\sqrt{s_{\mathrm{NN}}} = 3.0\,\mathrm{GeV}$ is found to scale with the mass number, consistent with hypernuclei formation via coalescence.

REFERENCES

[1] F. Hildenbrand and H.-W. Hammer, Phys. Rev. C **102**,064002(2020)
[2] M. S. Abdallah et al. (STAR Collaboration), Phys. Rev. Lett. **128**,202301(2022)
[3] A. Gal and H. Garcilazo, Phys. Lett. B **791**,48(2019)
[4] A. Gal, EPJ Web Conf. **259**,08002(2022)
[5] J. Adam et al. (ALICE Collaboration), Phys. Lett. B **754**,360(2016)
[6] A. Andronic et al., Phys. Lett. B **697**,203(2011), (update, preliminary)
[7] S. Zhang et al, Phys. Lett. B **684**,224(2010)